Lattice effects in $La_{1-x}Ca_xMnO_3$ ($x=0 \rightarrow 1$):
Relationships between distortions, charge distribution, and magnetism

C. H. Booth*

*Department of Physics and Astronomy, University of California, Irvine, California 92697
and Physics Department, University of California, Santa Cruz, California 95064*

F. Bridges

Physics Department, University of California, Santa Cruz, California 95064

G. H. Kwei

Los Alamos National Laboratory, Los Alamos, New Mexico 87545

J. M. Lawrence

Department of Physics and Astronomy, University of California, Irvine, California 92697

A. L. Cornelius and J. J. Neumeier†

Los Alamos National Laboratory, Los Alamos, New Mexico 87545

X-ray-absorption fine-structure measurements from the Mn and La K edges of samples of $La_{1-x}Ca_xMnO_3$ ($x=0 \rightarrow 1$) are presented as a function of temperature. In the insulating state, distortions of the Mn-O environment are found to be linear with calcium concentration x. These distortions are consistent with a model where individual Mn^{3+} sites have strong Jahn-Teller (JT) distortions while Mn^{4+} sites do not, although intermediate distortions are also possible. Comparisons to simulations of various possible bond length distributions show that these distortions are best modeled as a JT distortion, as opposed to charge disproportionation or other models. In the metallic state, at least $\sim 70\%$ of the distortion is removed. A similar effect is seen in the Mn-Mn bond length distribution. The La-O bond length distribution does not change significantly through the ferromagnetic transition, constraining possible changes in the Mn-O-Mn bond angle to less than 0.5°. The changes in the MnO_6 distortion that occur near T_c are also present (to a lesser degree) in an insulating sample with $x=0.12$. The functional relation between the MnO_6 distortions and the magnetization is determined, and compared to transport measurements. [S0163-1829(98)04917-0]

I. INTRODUCTION

The $La_{1-x}A_xMnO_3$ series (where A is a divalent metal such as Ca, Sr, Ba, or Pb) demonstrates many interesting electronic, magnetic, and structural properties. Stoichiometric $LaMnO_3$ has a distorted perovskite structure and Mn^{3+} is Jahn-Teller (JT) active. Below a Néel temperature T_N, the system is also an antiferromagnetic (AF) insulator, with ferromagnetic (FM) coupling within MnO_2 planes and AF coupling between the planes.[1] At room temperature, systems with $A=Ca$ are paramagnetic (PM) insulators. For $0 < x \lesssim 0.2$, these systems have a FM transition at a Curie temperature T_c, and are also insulators. For $0.2 \lesssim x \lesssim 0.48$, these materials have a FM transition which coincides with a metal-insulator (MI) transition.[2–4] At higher calcium concentrations, the system becomes antiferromagnetic below T_N and is an insulator both above and below T_N. This region of x also exhibits charge ordering (CO).[5,6] A large peak in the magnetoresistance (MR) was measured in $La_{0.8}Sr_{0.2}MnO_3$ near room temperature by Volger.[7]

The basic mechanism of electronic transport has long been thought to be the "double-exchange" (DE) mechanism,[8–10] whereby an electron requires less energy to hop to a neighboring Mn site if the spin of the ion at that neighboring site is aligned with the electron's spin. Such a hopping also promotes ferromagnetic order in the lattice. Although DE correctly predicts many of the properties of these materials, detailed calculations of the electronic properties must account for spin-lattice interactions.[10] Recent reexaminations of the material have dubbed the magnetoresistance effects in these materials "colossal" magnetoresistance (CMR) because of the enhancements of the effect that can be obtained in thin films, by varying the stoichiometry, and by high applied magnetic fields.[11–14] These enhancements cannot be understood only in terms of the DE model: In many cases, the magnetoresistance generated by the DE model is much smaller than is actually measured.[15] One possibility for understanding the large magnetoresistance is to allow for a large lattice distortion above T_c, which is at least partially removed below T_c.[16–19] This distortion would occur when a localized charge carrier induces a polaron distortion, which increases the energy required for the charge to hop to a neighboring site.

There is a growing body of literature supporting a strong spin-lattice coupling in these materials. In particular, an orthorhombic to rhombohedral transition can be driven with an applied magnetic field,[20] and a large isotope shift of T_c

($\sim$20 K) with high O^{18} concentration has been measured.[21] Evidence supporting polaronic transport above T_c includes resistivity[22] and thermoelectric power[23] (TEP) measurements. Perhaps the most convincing studies showing a connection between the electronic properties and the lattice are the local-structure measurements which show that the Mn-O environment orders sharply as the temperature is decreased through T_c, consistent with near-neighbor Mn-O bond lengths separated by $\sim$0.1 Å above T_c that are less separated below T_c.[24-27] The order of magnitude of these distortions was predicted by Millis *et al.*,[17] and is consistent with the size of the JT distortion in LaMnO$_3$. Changes in the oxygen thermal parameters at T_c measured by diffraction[28-30] confirm that the oxygen atoms are involved in the CMR transition.

Although the importance of the spin-lattice interaction has now been well established, several fundamental questions remain. Many such questions can be elucidated by a local-structure probe. One important issue for understanding the resistivity above T_c, and hence the size of the magnetoresistance, is to determine how much of the distortion is removed below T_c. It has been shown from x-ray-absorption fine-structure (XAFS) analysis that the polaron below T_c is not completely delocalized in CMR samples of La$_{1-x}$Ca$_x$MnO$_3$, since the distortion of the Mn-O pairs still decreases with increasing magnetization.[26] Likewise, pair-distribution function (PDF) analysis of neutron diffraction data has demonstrated that the size of the distortion in CMR samples of La$_{1-x}$Sr$_x$MnO$_3$ is intermediate between completely localized and itinerant.[27] These PDF data have been interpreted as indicating that the distortion is spread out over approximately three Mn sites.[27] Further work is needed to clarify the nature of the distortion, and in particular how it is related to other properties of the materials.

Another central issue concerns the driving force for polaron formation. A strong possibility is that when no hole resides on a Mn lattice position, that is, the Mn is in the 3+ state, a local JT distortion is generated around that site. Certainly the overall size of the distortion is consistent with a JT distortion. However, other possibilities exist. For instance, if a large fraction of the Mn^{3+} charge-disproportionates (CD) into Mn^{2+} and Mn^{4+}, similar distortions would be created. In such a model, the fractional amount of CD changes with calcium concentration x. This model is supported by thermogravimetric and equilibrium constant work[31,32] and TEP (Ref. 33) measurements. We will consider these and other possible models of the distortions by comparing them to the measured distortions as a function of x, and in particular, to the distortions in the end members LaMnO$_3$ and CaMnO$_3$.

All local-structure studies to date have shown changes in the distribution width of the Mn-O pairs as T passes through T_c. These results are very strong evidence for small polaron formation above T_c mediated by localized (on the time scales of phonons) electrons converting Mn^{4+} to Mn^{3+}. However, the nature of local probes is that they only measure radial distances between atoms. It has been suggested that the Mn-O-Mn bond angle may play the more significant role, since this angle determines the matrix element for hopping between Mn sites.[34] Previous structural studies did not address changes in the Mn-O-Mn bond angle. In fact, a change in the Mn-O bond length distribution width (as in Refs. 24–27)

could be a consequence of a change in the Mn-O-Mn bond angle. If such a change in the bond angle occurs, it should result in significant changes in the Ca-O or La-O bond lengths ($\sim$0.2 Å). If this change in angle were the only effect, PDF measurements[24,27] likely would have measured it. On the other hand, if the changes in the Mn-O-Mn angle were somewhat smaller, PDF analysis may have had trouble detecting it, since the O-O, Ca-O, and La-O peaks all fall on top of each other. (Large changes in this peak were attributed solely to changes in the O-O distribution.) A less ambiguous measurement of the direction of the oxygen distortion is thus vital for determining the mechanism allowing for metallic-like transport.

Last, obtaining some more quantitative relations between the structural, magnetic, and electrical properties could be an important step towards understanding the physics of the CMR materials. For instance, Hundley *et al.*[22] have shown that the resistance and the magnetism relate simply by $\ln(\rho)\propto-M$. Cohn *et al.*[35] have found that the lattice thermal resistivity scales with MnO$_6$ distortions for various samples of La$_{1-x}$Ca$_x$MnO$_3$, and that the total thermal resistivity κ^{-1} goes as $K_1-K_2M^2$ (K_1 and K_2 are constants) for $A_x=$Sr$_{0.17}$. As shown in Ref. 26, the temperature dependence of the disorder of the Mn-O in the metallic state is likely related to the magnetism, rather than thermal effects. We have recently shown that a simple model of the distortions can yield an effective delocalized hole concentration n_{dh}, and that $\ln(n_{\text{dh}})\propto M$.[36] Here we present a more detailed analysis of this result and compare with other possible models.

In order to directly address these and other questions, we have performed XAFS experiments on the La$_{1-x}$Ca$_x$MnO$_3$ series ($x=0\rightarrow1$) from $T=50$ K to 300 K. Mn K-edge data allow us to measure various properties of the MnO$_6$ distortion, including changes in the Mn-Mn bond length distribution near T_c. La K-edge data allow us to measure any possible changes in the Mn-O-Mn bond angle by isolating the La-O bonds. Comparisons of the samples with various x allow us to determine how much of the distortion is really removed in the magnetic state. In Sec. II we describe the experimental setup and basic sample characterization. We present the absorption and XAFS data in Sec. III, and analyze the results in terms of various distortion models and changes with magnetization in Sec. IV. Our results are summarized in Sec. V.

II. EXPERIMENTAL DETAILS

Powder samples of La$_{1-x}$Ca$_x$MnO$_3$ ($x=0.0$, 0.12, 0.21, 0.25, 0.3, 0.65, and 1.0) were prepared by solid state reaction of La$_2$O$_3$, CaCO$_3$, and MnO$_2$ with repeated grindings and firings at temperatures up to 1400 °C and a final slow cool at 1 °C per minute. The dc magnetization was measured using a commercial superconducting quantum interference device (SQUID) magnetometer. Samples with $x=0.0$ and 1.0 showed antiferromagnetic transitions at $\sim$130 and 125 K, respectively. The magnetization of the $x=0.65$ sample showed features consistent with a CO transition at 270 K and an AF transition at $\sim$140 K.[5,6] Diffraction measurements of the LaMnO$_3$ sample indicate that this sample is monoclinic, while all other samples are orthorhombic. TGA shows the actual stoichiometry of this sample to be LaMnO$_{3.006}$. Figure
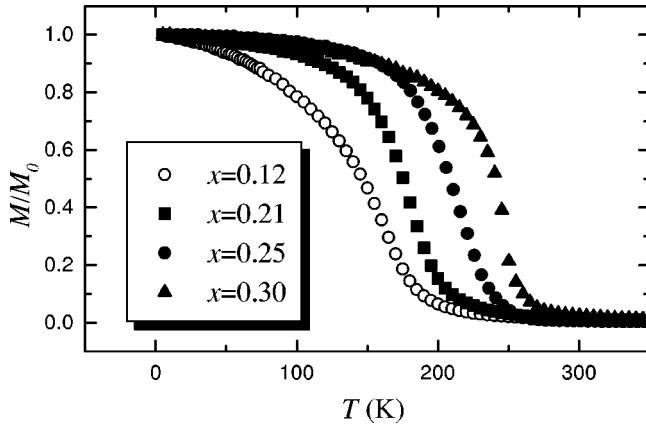
FIG. 1. Normalized magnetization vs T for the ferromagnetic samples of $La_{1-x}Ca_xMnO_3$. These data are normalized to the magnetization at $T=5$ K, M_0. All data were collected at 5000 Oe, except for $x=0.25$, which were collected at 1500 Oe.

FIG. 2. A single XAFS scan of $k\chi(k)$ vs k for $La_{0.75}Ca_{0.25}MnO_3$ at $T=50$ K, as an example of data quality.

1 shows the magnetization for the ferromagnetic samples, $x=0.12$, 0.21, 0.25, and 0.30. T_c's are estimated to be 198(2), 210(2), 243(2), and 260(2) K, respectively, by extrapolating the data at maximum slope to $M=0.0$. The transition of the insulating $x=0.12$ sample is much broader than the other FM samples, all of which have CMR transitions in the vicinity of T_c. This sharpening of the transition in the presence of the CMR transition may be a sample-dependent effect, or may be due to DE enhancement of the magnetism.

All XAFS data were collected at the Stanford Synchrotron Radiation Laboratory (SSRL). Mn K-edge data were collected on beam line 2-3 using Si(220) double monochromator crystals for all samples. La K-edge data were collected on beam line 4-2 using Si(400) crystals for samples with $x=0.12$, 0.21, 0.25, and 0.65. All data were collected in transmission mode. A powdered Mn metal sample was used as an energy reference for the Mn K-edge data. The manganite powders were reground, passed through a 400-mesh sieve, and brushed onto Scotch tape. Layers of tape were stacked to obtain absorption lengths $\mu_{Mn}t\sim1$ for each sample. Samples were placed in an Oxford LHe flow cryostat, and temperatures were regulated to within 0.1 K. Absorption from other excitations (pre-edge absorption) was removed by fitting the data to a Victoreen formula, and a simple spline (7 knots at constant intervals ~140 eV in E) was used to simulate the embedded-atom absorption μ_0. The XAFS oscillations χ were then obtained as a function of photoelectron wave vector $k=\sqrt{2m_e(E-E_0)/\hbar^2}$ from $\chi(k)=\mu/\mu_0-1$. E_0 of the samples was determined from the first inflection point of the main edge, with E_0 of Mn metal set to 6539 eV. Fits to the data were performed in r space after Fourier transforming (FT) $k\chi(k)$. The real and imaginary parts of this transform are complicated functions of the scattering potentials. We fit to backscattering amplitudes and phases calculated by the FEFF6 code,[37] which has been shown to be very accurate over a wide range of materials (for instance, see Ref. 38). XAFS amplitudes are subject to an overall reduction factor S_0^2, which can be determined well from a suitable model compound. All fits reported for the Mn K edge use an $S_0^2=0.72$, obtained from $CaMnO_3$. Further details of the methods used to reduce and fit the data can be found in Ref. 38.
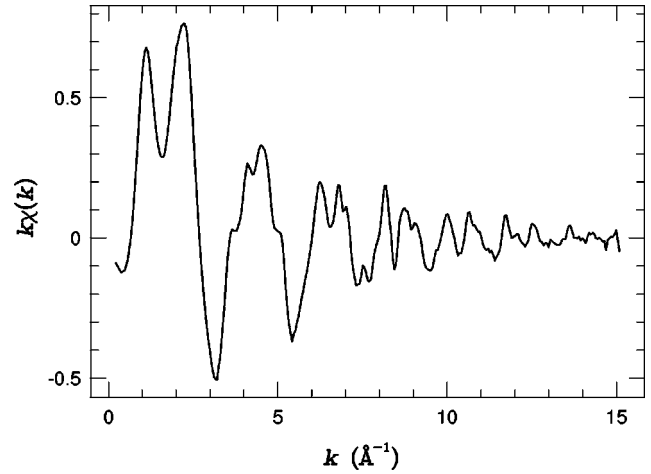
Figure 2 shows $k\chi(k)$ vs k for $La_{0.75}Ca_{0.25}MnO_3$ as an example of data quality.

Generally, three scans were collected at each temperature point for each sample, although occasionally only two were obtained. Estimated errors reported below are based on the reproducibility of these scans to emphasize relative changes in the material from one temperature to the next, and in no way account for absolute errors. Absolute errors on nearest-neighbor bond lengths for well-ordered reference crystals have been shown to be ~0.005 Å.[38] Errors in bond length distribution widths (σ) are around 5% for nearest neighbors, but can be as high as 20% for further neighbors with intervening atoms, such as Mn-O-Mn. Relative errors, that is, measurements of changes in the amplitudes and bond lengths from one temperature to the next, are much better because the main contribution to such errors is from counting statistics, rather than from the fitting function.

The relative errors from one temperature to the next have been minimized by carefully checking the alignment of the sample to the incident photon beam. The vertical sample profile was scanned at each temperature and data collected on the same point on the sample. Checking this alignment is important due to thermal contraction of the sample holder. Generally, the sample was aligned within ~50 μm. Cases where such good alignment was not obtained are reflected by larger estimated errors in the plots.

III. RESULTS

A. Valence determinations from edge region

The absolute photoelectron excitation energy can give a good measure of the mean Mn valence, provided a suitable reference material can be obtained. We used $LaMnO_3$ and $CaMnO_3$ as the Mn^{3+} and Mn^{4+} reference standards, respectively. E_0, as measured from the inflection point in the main part of the edge (Fig. 3), was found to be 4.15(10) eV higher for $CaMnO_3$ than $LaMnO_3$, in agreement with Subías *et al.*[39] All Ca-substituted samples had E_0's that agreed with a simple linear interpolation of the Mn^{3+} and Mn^{4+} standards based on calcium concentration within an experimental error of 0.06 valence units (0.2 eV) for each measured tempera-
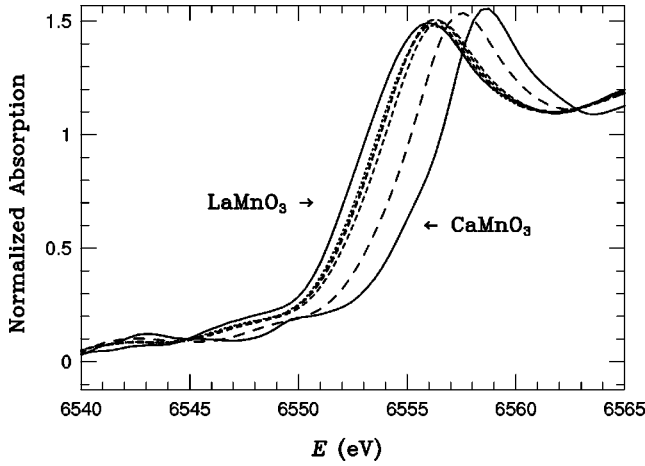
FIG. 3. Main absorption edge μt vs E for all samples at T = 50 K. The absorption jump at the threshold energy E_0 (energy at inflection point), as determined by a Victoreen formula, is normalized to unity. From left to right, the samples are $x=0.0$ (solid line), $x=0.12$ (dotted line), $x=0.21$, 0.25 and 0.30 (short dashed line), $x=0.65$ (long dashed line), and $x=1.0$ (solid line).

ture. Likewise, no changes in edge position with temperature were observed for any of the samples, within experimental error.

Interestingly, the *slope* of the main edge does not change much across the entire concentration range. If individual Mn^{3+} and Mn^{4+} sites exist, one would expect the slope of the main absorption edge to broaden for intermediate dopings, i.e., $x\sim0.5$. This effect should be observable in the x = 0.65 data. No significant change in the slope is measured for this sample, indicating that the Mn acts mixed valent on these time scales ($\sim10^{-15}$ s) despite the fact that this sample is a charge-ordered insulator. Further work is needed to understand the significance of this result.

By averaging all the measurements above T_c and those below T_c for each sample, we find no shift in the edge energy from 300 K to 50 K to within 0.02 eV, or 5×10^{-3} valence units. This averaged measurement disagrees with Ref. 25, which reports an increase of the Mn K-edge energy of 0.5 eV as the temperature is lowered through T_c in a sample of La$_{0.67}$Ca$_{0.33}$MnO$_3$. This large measured difference may be due to the much smaller amount of data used in Ref. 25. For instance, our measurement of La$_{0.7}$Ca$_{0.3}$MnO$_3$ includes 32 scans over 11 temperatures, whereas Ref. 25 used 11 scans over 3 temperatures. Even so, this large discrepancy is outside the estimated error for both experiments.

It is worth noting that for La$_{0.6}$Y$_{0.07}$Ca$_{0.33}$MnO$_3$ (T_c =160 K), Subías *et al.*[39] have measured a small edge shift of $\sim+0.01$ eV between 210 K and 50 K. In addition, they measure a positive shift of $\sim+0.10$ eV between 210 K and 160 K and a shift of ~-0.09 eV from 160 K to 50 K. These authors report that they obtain similar results for La$_{0.67}$Ca$_{0.33}$MnO$_3$. Our experiments are not sensitive enough to unambiguously detect to such small shifts.

B. Local structure of the end members LaMnO$_3$ and CaMnO$_3$

LaMnO$_3$ and CaMnO$_3$ have essentially the same structure: Each is a distorted perovskite with canted MnO$_6$ octahedra that create Mn-O-Mn bond angles within $\sim2°$ of

TABLE I. Near-neighbor bond lengths R and number of neighbors, N, for various atom pairs in LaMnO$_3$ and CaMnO$_3$ as given by diffraction studies (Refs. 40–42). Data for individual bond lengths are averaged to account for the poorer resolution of XAFS data for these pure materials. The LaMnO$_3$ sample Norby *et al.* (Ref. 40) used was orthorhombic, while Mitchell *et al.* (Ref. 41) had a monoclinic sample. The monoclinic sample was found to have four distinct Mn sites. We have averaged the atomic pair distances of these sites for this table. Similarly, the Mn-Ca/La environments for these materials are very distorted, and so their average bond lengths are also reported here.

	LaMnO$_3$[a]		LaMnO$_3$[b]		CaMnO$_3$[c]	
Atom pair	N	R	N	R	N	R
Mn-O	2	1.92	2	1.91	6	1.90
	2	1.97	2	1.97		
	2	2.15	2	2.17		
La/Ca-O	4	2.45	4	2.45	4	2.35
	4	2.7	4	2.67	4	2.57
	4	3.2	4	3.3	4	3.0
Mn-Ca/La	2	3.24	2	3.24	2	3.09
	4	3.39	4	3.38	4	3.23
	2	3.65	2	3.67	2	3.37
Mn-Mn	2	3.86	6	3.98	6	3.73
	4	3.97				

[a]Reference 40.
[b]Reference 41.
[c]Reference 42.

159°.[40–42] Consequently, the unit cell is larger than the simple cubic unit cell containing one formula unit. Both La and Ca are distorted from the central position in the simple cubic unit cell, making their near-neighbor oxygen environment complicated. In addition to these distortions, LaMnO$_3$ has a JT distortion which splits the six otherwise equal (within 0.01 Å) Mn-O bond lengths in the tilted octahedra into three pairs of unequal length. This distortion preserves (within a couple degrees) the Mn-O-Mn bond angles. Table I lists some of the important bond lengths as given by the diffraction studies.

Figure 4 shows the FT of $k\chi(k)$ vs r of both these compounds at $T=50$ K from the Mn K-edge data. Also shown in this figure is a simulation (i.e., no free parameters) using the structures from Ref. 41 and Ref. 42, calculated by FEFF6.[37] The simulations use a correlated Debye model with a Debye temperature $\Theta_D=550$ K [specific heat of LaMnO$_3$ gives $\Theta_D=300$ K (Ref. 43)]. The reader should note that the correlated Debye temperature describes the thermal dependence of the bond length distribution width for *pairs* of atoms. Since bond lengths are not very sensitive to acoustic phonon vibrations, estimates of the correlated Debye temperature are often higher than the (uncorrelated) Debye temperature obtained from heat capacity or diffraction measurements.

The amplitude of the complex transform gives a measure of the number of neighbors to the Mn atoms at a given r. The real part of the transform (sometimes referred to loosely as the ''phase'') is very sensitive to shifts in the atom-pair separation distances. Both the amplitude and the phase are sensitive to the species of neighboring atom. The position of
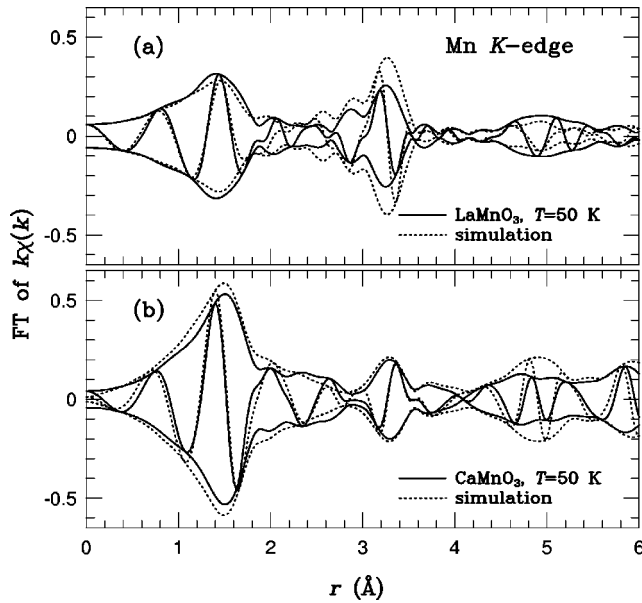
FIG. 4. Mn K-edge Fourier transforms (FT's) of $k\chi(k)$ vs r for (a) LaMnO$_3$ and (b) CaMnO$_3$ at $T = 50$ K. The oscillating curve is the real part of the transform and the outer envelope is the amplitude of the transform ($[Re^2 + Im^2]^{1/2}$). The dotted line in each panel is a simulation using diffraction data from Mitchell *et al.* (Ref. 41) for LaMnO$_3$ and Poeppelmeier *et al.* (Ref. 42) for CaMnO$_3$. The simulations are calculated using FEFF6 (Ref. 37). All transforms in this paper are from 3.5 to 14.5 Å^{-1} and Gaussian broadened by 0.3 Å^{-1}.

peaks in the amplitude are shifted from the actual interatomic pair distances by a phase shift due to the scattering of the photoelectron from both the central and the neighboring atoms. Since the FT has real and imaginary parts, contributions from different scattering paths can constructively or destructively interfere. Fits to the (calculable) contribution from individual atom pairs are therefore necessary to get reliable detailed information about the local structure. In any case, the first peak at ~ 1.5 Å is due to the near-neighbor Mn-O bond lengths near 1.97 Å. The "multipeak" from ~ 2.6 to 3.5 Å has contributions from Mn-La, Mn-Ca, and Mn-Mn paths (see Table I for actual bond lengths), including the multiple scattering contributions from Mn-O-Mn paths.

The agreement between the data and the simulations is remarkable, indicating that the local structure around Mn in these samples is very similar to the average structure given by the diffraction data used to calculate the simulations. We must point out that the structure used in the simulations of Fig. 4 for LaMnO$_3$ are from Ref. 41, which finds a space group of $P2_1/c$, in agreement with diffraction data on our sample. A simulation using data from Ref. 40, which uses the *Pnma* space group (indicating excess oxygen[41]), compares just as well to the XAFS transform. In fact, the simulations from Ref. 40 and Ref. 41 are almost identical for atom-pair separations that are as long as the Mn-Mn pairs. Therefore, these Mn K-edge XAFS experiments are not sensitive to the changes in local structure arising from the differences between the stoichiometric (monoclinic) and off-stoichiometric (orthorhombic) samples. On the other hand, simulations using data from Elemans *et al.*[44] do not compare well with the XAFS results. (See Sec. III D for comparisons at the La K edge.)
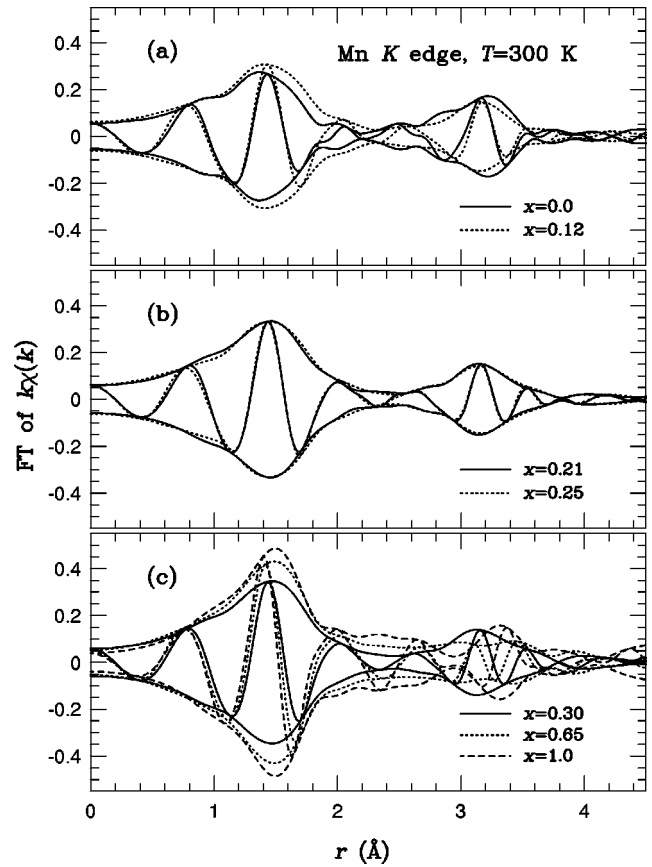

FIG. 5. FT of $k\chi(k)$ vs r for all samples at $T = 300$ K. These transforms are related to the radial-distribution function. Peaks in amplitude correspond to neighbors around Mn atoms. Peak positions correspond to bond lengths up to an overall phase shift that corresponds to the species of the neighbor. For instance, the first peak at 1.5 Å corresponds to the Mn-O distances ~ 1.95 Å.

The amplitude of the first peak is most sensitive to the coordination number and distribution width of the nearest-neighbor oxygens. Sensitivity to long Mn-O bonds is lower than to short Mn-O bonds because the XAFS amplitude falls off as $1/r^2$. In the case of the CaMnO$_3$, this first peak corresponds to all six Mn-O pairs at a distance of ~ 1.9 Å. Since the Mn-O environment in LaMnO$_3$ is JT distorted, this first peak is mostly sensitive to the first two Mn-O lengths at ~ 1.92 Å and 1.97 Å, and less sensitive to the long Mn-O bonds at ~ 2.18 Å. Differences between the simulation and the data near 1.95 Å in the LaMnO$_3$ spectrum are likely due to differences between our sample and the model for this longer Mn-O peak.

Results of fits to these data are reported below in the context of the La$_{1-x}$Ca$_x$MnO$_3$ series.

C. La$_{1-x}$Ca$_x$MnO$_3$ series from the Mn K edge

Figure 5 shows the FT of $k\chi(k)$ for the Mn K-edge data for the full La$_{1-x}$Ca$_x$MnO$_3$ series at $T = 300$ K, which is above any magnetic transitions in all the samples. LaMnO$_3$ and CaMnO$_3$ data are shown here again (at a higher temperature) for comparison. As the calcium concentration is increased to $x = 0.12$, the first Mn-O peak (at 1.5 Å) grows and the combined Mn-La/Ca and Mn-Mn multipeak (at ~ 3.2 Å) becomes smoother. The increase of the Mn-O peak ampli-
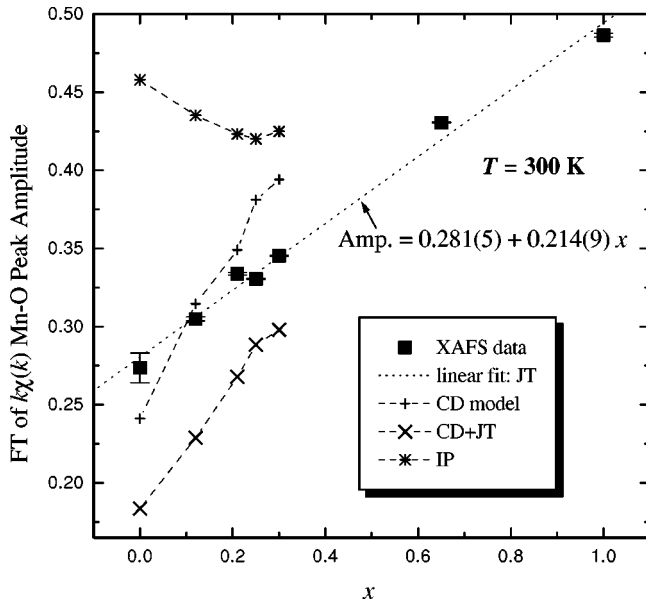
FIG. 6. Amplitude of the Mn-O peak vs x at 300 K. Generally, the amplitude decreases with increasing distortions or disorder ($\sim 1/\sigma$ for harmonic distributions). Simulations of possible models of the distortions are also displayed (please see text). Error bars in this and subsequent plots represent reproducibility, and do not account for systematic errors.

FIG. 7. Amplitude of the Mn-O peak vs x at 50 K (well below any T_c's). For the non-CMR materials, the conclusion from Fig. 6 still holds; i.e., the Mn-O environment acts like a weighted average of the LaMnO$_3$ and CaMnO$_3$ structures (see the text for discussion of $x=0.12$ amplitude). The open-box symbol shows roughly the amplitude LaMnO$_3$ would have if it were not JT active (see the text). The CMR Mn-O amplitudes are between the linear interpolations from CaMnO$_3$ to either LaMnO$_3$ or the modeled non-JT LaMnO$_3$. These data indicate that the JT distortion is clearly smaller below T_c in the CMR materials, but it is only $\sim 70\%$ removed.

tude indicates that the oxygen environment around the manganese is becoming less distorted; i.e., at least part of the significant distortion in LaMnO$_3$ is removed. The smoother Mn-La/Ca and Mn-Mn multipeak indicates that the distribution of bond lengths is probably becoming more ''continuous;'' that is, the bond length distribution is becoming more disordered rather than distorted with distinct bond lengths. This smoothing of the Mn-La/Ca and Mn-Mn multipeak is even more dramatic at $T=50$ K (Fig. 4 shows LaMnO$_3$ at $T=50$ K; other concentrations are qualitatively the same as at 300 K in Fig. 5 for these peaks). As x is increased to 0.21, 0.25, and 0.3, the Mn-O peak continues to grow and the Mn-La/Ca and Mn-Mn environment does not change appreciably. The $x=0.65$ sample breaks this trend, with a very different La, Ca, and Mn environment, although the Mn-O peak has continued to grow with x. The amplitude near 2.4 Å in the transforms grows noticeably in the $x=0.65$ sample. This region in the CaMnO$_3$ spectra is even larger in amplitude. The peak at 3.2 Å in the CaMnO$_3$ transform is similar in amplitude to the other materials, but $\sim 180°$ out of phase (real part) compared with the corresponding peak for LaMnO$_3$ (see Fig. 4) and the CMR materials. This is the result of very different backscattering functions for La and Ca. The $x=0.65$ sample is an intermediate case; the phase is shifted, relative to LaMnO$_3$, but much less than $180°$. Since this peak is a weighted sum of contributions from Mn-Ca and Mn-La, such a phase shift is expected for this sample, and does not indicate any large changes in the local structure in this bond length range with x.

1. Amplitude of Mn-O Fourier transform peak

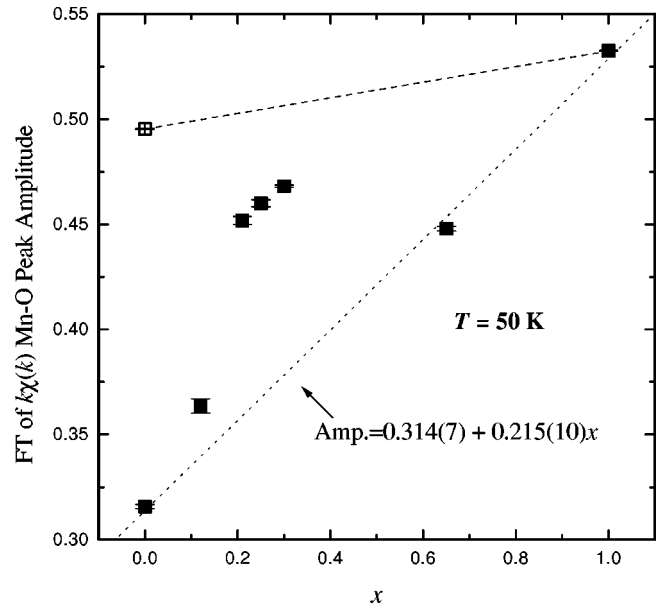We will now focus on the amplitude of the Mn-O peak in the transformed data. First consider the room temperature

data, which is above any magnetic transitions (same temperature as presented in Fig. 5). The amplitudes of the Mn-O peak in the transforms are well described ($\sim 3\%$) by linearly interpolating the amplitudes from LaMnO$_3$ and CaMnO$_3$ based on the Ca concentration (Fig. 6). This indicates that the oxygen environment around manganese in Ca-substituted samples acts like a linearly interpolated average of the two end members. This result will be discussed in detail in Sec. IV A 2.

For the materials with a CMR transition, the Mn-O environment orders as the systems become ferromagnetic, but some disorder exists even in the metallic state. Figure 7 shows the Mn-O peak amplitude at 50 K. The samples without a CMR transition still fall on a line that includes the end compounds, with the same slope as at room temperature. The CMR samples fall well above this line, indicating that at least some of the distortion present above T_c has been removed. A possible exception is the $x=0.12$ sample: A reasonable linear fit can be obtained while including this sample, but it appears that the MnO$_6$ distortions are partially removed in the FM state in this sample as well as in the CMR samples. We will discuss this result further below.

We can determine whether all of the distortion has been removed by comparing to the amplitude if no distortions were present. If the MnO$_6$ octahedra were not distorted in LaMnO$_3$, that is, if the Mn-O bond lengths in LaMnO$_3$ were equal (within ~ 0.03 Å or so), we expect that the amplitude of the first peak would be slightly smaller than in CaMnO$_3$. This decrease occurs because XAFS amplitudes are propor-

tional to $1/r^2$. The unit cell of LaMnO$_3$ is inherently larger than that of CaMnO$_3$ and thus the Mn-O bond length would be ~ 0.07 Å longer for Mn^{+3}, relative to that for Mn^{+4} in CaMnO$_3$. We therefore expect to get an amplitude for "undistorted" LaMnO$_3$ shown by the open square in Fig. 7. Likewise, if all the Mn-O bond lengths within the MnO$_6$ octahedra for the CMR samples were the same in the metallic state, we would expect the Mn-O amplitude for these samples to roughly fall on a line intermediate between LaMnO$_3$ (no JT distortion) and CaMnO$_3$. As Fig. 7 shows, the Mn-O amplitude for the CMR samples falls well below such a line. This analysis suggests that DE below T_c removes only about 70% of the distortion above T_c. The residual width of the Mn-O bond length distribution may be due to persisting static distortions or from dynamic fluctuations of the lattice. These possibilities will be discussed in Sec. IV C. (It should be noted that the discussion above is somewhat qualitative because the amplitude is assumed to be proportional to the pair-distribution amplitude. However, the amplitude of XAFS data includes the interference effects, and therefore the above discussion is limited to distortions $\lesssim 0.1$ Å.)

2. Fits to Mn K-edge data

Fits were performed to the Mn K-edge data in order to quantify the changes in the local structure with temperature. Since XAFS cannot fully resolve any possible JT or similar distortions (even in LaMnO$_3$), we fit the data with a simplified model which includes single Gaussian distributions for the 6 Mn-O, $8(1-x)$ Mn-La, $8x$ Mn-Ca, and 6 Mn-O-Mn scattering paths. Including more detail (i.e., three separate Mn-O paths to try and fit the distortion) resulted in higher-quality fits, but the results were not unique. In this model, the distortion will be accounted for by a broad Mn-O bond distribution width (correlated Debye-Waller factor σ). Figure 8 shows $\sigma^2_{\text{Mn-O}}$ as a function of temperature. (Recall that the small error bars show the relative errors, as discussed in Sec. II.) The LaMnO$_3$ and CaMnO$_3$ distribution widths are consistently the highest and the lowest (respectively) of the series at all temperatures. All the insulating materials exhibit a gradual increase in $\sigma^2_{\text{Mn-O}}$, consistent with thermal broadening, i.e., the correlated Debye model. Above T_c, $\sigma^2_{\text{Mn-O}}$ for the CMR materials appears to have this standard thermal temperature dependence. As these samples become ferromagnetic, the Mn-O distribution narrows. There is also some evidence in Fig. 8 of a slight narrowing for the $x=0.12$ sample.

Even well below T_c where the magnetization is nearly saturated, the distribution gets narrow faster than a thermal model would allow: Fits to a correlated Debye model for these samples well below T_c (first 2–3 points) require an unphysical, negative static distortion. More specifically, the increase in curvature between the fits to $\sigma^2_{\text{Mn-O}}$ for the $x=0.0$ and the $x=0.30$ data suggests at least a 20% decrease in Θ_D. Since the correlated Debye model gives $\sigma^2(T=0$ K$)\propto 1/\Theta_D$, we would expect a $\sim 20\%$ increase in $\sigma^2_{\text{Mn-O}}$ at low T. Such an increase is not observed. This result is consistent with our previous measurements,[26] which caused us to conjecture that well below T_c, changes in the Mn-O distribution are primarily governed by changes in the mag-
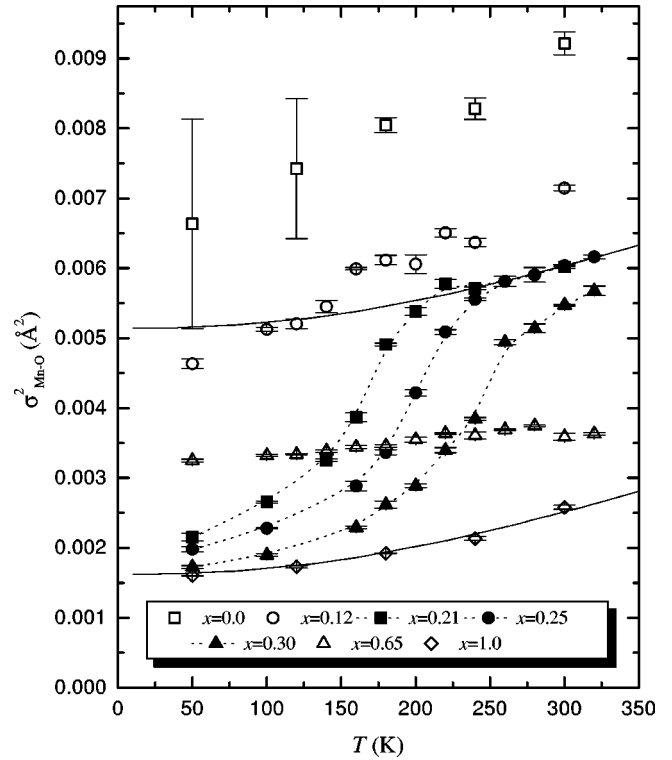

FIG. 8. Correlated Debye-Waller width parameters σ^2 for the Mn-O distribution vs T. Open symbols are for materials without the CMR transition, while solid symbols correspond to materials with a CMR transition. The insulators' widths increase with temperature consistent with thermal broadening. The distribution width of the Mn-O bonds for CaMnO$_3$ is described well with a correlated Debye model and $\Theta_D=940\pm30$ K (solid lines). This same model with an additional 0.0043 Å^2 static broadening also describes the high-temperature data for $x=0.21$ and 0.25, and was previously shown to describe data from La$_{0.5}$Ca$_{0.5}$MnO$_3$. (Ref. 26). The $x=0.65$ widths are more consistent with a $\Theta_D=1100\pm100$ K. The Debye temperatures for $x=0.0$ and 0.12 are less clear, but are greater than 600 K. The width of the CMR samples changes rapidly with temperature near T_c. Dotted lines are guides to the eye.

netization. This possibility is considered in detail for all the CMR samples in Sec. IV C.

Figure 9 shows the weighted average Mn-O bond lengths $R_{\text{Mn-O}}$. Recall that we have chosen to quantify the XAFS results with a single Gaussian distribution because XAFS cannot resolve all the Mn-O peaks in this distorted environment. By using this distribution, we are more sensitive to the nearest Mn-O neighbors around 1.95 Å because of the $1/r^2$ factor than to the Mn-O neighbors near 2.15 Å. Hence, for a material with a JT or CD-type of Mn-O distortion that grows as the temperature is increased, we expect that the weighted average bond length measured by XAFS will decrease. This decrease occurs because, in the case of a JT distortion, two Mn-O bonds shorten, two lengthen, and two do not change (to first order). The higher sensitivity to shorter bonds results in a shortening of the average bond length as measured by XAFS.[45] Consequently, changes in the measured bond length would indicate in this case a change in the *distribution* of bond lengths, rather than an actual change in the bond length for any particular atom pair. CMR materials all exhibit a shrinking of the Mn-O bond, commensurate with the de-
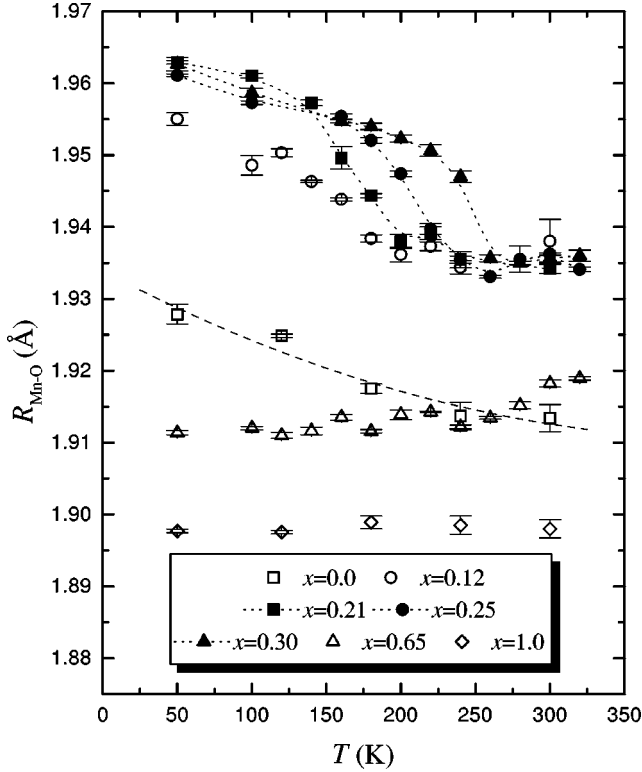
FIG. 9. $R_{\text{Mn-O}}$ vs T. $R_{\text{Mn-O}}$ is the measured Mn-O bond length, using a single Gaussian Mn-O distribution to fit the nearest-neighbor environment. In the event of an anharmonic distortion (such as a JT distortion) XAFS measurements of average bond lengths will be lower than the actual mean of the distribution. Decreases in bond length with temperature may therefore indicate an increase of anharmonic distortions in this system. The dashed line is a polynomial fit to $R_{\text{Mn-O}}$ for LaMnO$_3$, as a guide to the eye.

FIG. 10. $\sigma^2_{\text{Mn-Mn}}$ vs T for (a) insulating samples and (b) CMR samples. (Note that the $x=0.0$ and 0.21 data have been shifted by -0.002 Å^2 and $+0.003$ Å^2, respectively, to avoid overlap.) Data for CMR samples clearly show a step in $\sigma^2_{\text{Mn-Mn}}$ near T_c. Fits to data for $x=0.65$ were inconclusive regarding the Mn-Mn distribution width.

crease in magnetization. Interestingly, we measure a similar shrinking around T_c for the $x=0.12$ sample, indicating that some removal of the distortion may be occurring on a local scale in this material, even though it remains insulating. The continued lengthening of the mean Mn-O bond as T is lowered indicates that the decreasing distortions shown in Fig. 8 are closely related to a further removal of Mn-O distortions, even well below T_c. The LaMnO$_3$ material also shows a shrinking Mn-O distance with increasing temperature. We will discuss this unexpected result in Sec. IV B.

The other materials behave in a less unusual way. CaMnO$_3$ shows very little change of the Mn-O bond length of 1.898(2) Å with temperature (this Mn-O distribution should really be Gaussian; so these fits accurately describe the distribution) and the $x=0.65$ Mn-O bond length increases linearly from 1.912(2) Å to 1.919(2) Å.

Figure 10 shows $\sigma^2_{\text{Mn-Mn}}$ vs T. For the CMR samples these data show a very similar temperature dependence to the $\sigma^2_{\text{Mn-O}}$ data (Fig. 8), including a comparable decrease in width as T is lowered through T_c. Again for $x=0.12$, we observe a small decrease in disorder for $\sigma_{\text{Mn-Mn}}$ as T is lowered through T_c, similar to that observed for $\sigma_{\text{Mn-O}}$. In our previous study,[26] we measured a similar temperature dependence in samples with $x=0.25$ and 0.33, but we could not unambiguously assign this dependence to changes in the Mn-Mn atom-pair length distribution because changes in the
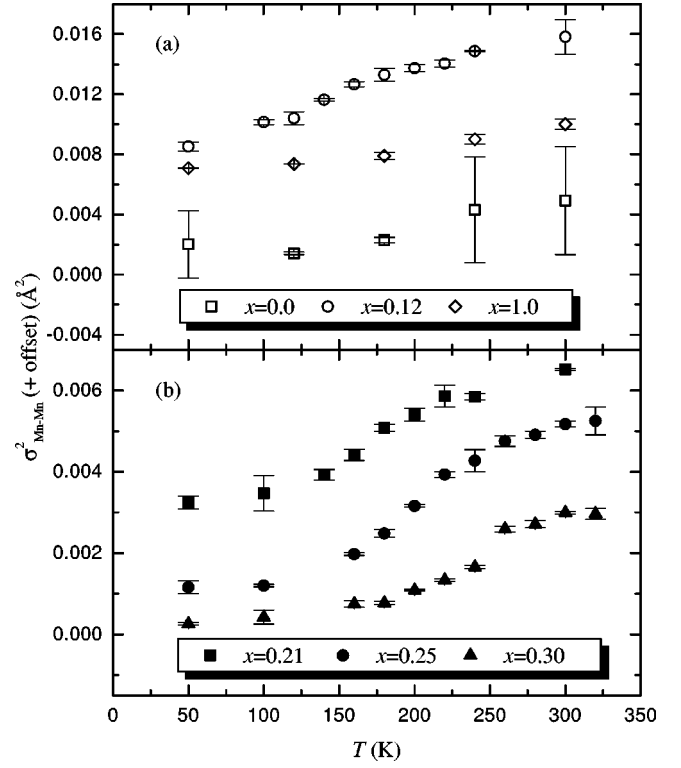
Mn-O-Mn bond angle could produce a similar effect. We rule out this possibility below.

D. La$_{1-x}$Ca$_x$MnO$_3$ series from the La K edge

La K-edge data were collected for the $x=0.12$, 0.21, 0.25, and 0.65 samples. The FT's of $k\chi(k)$ for these data are shown in Fig. 11. The first peak in the transform at ~1.8 Å includes contributions from all the La-O peaks listed in Table I, but primarily from the nearest eight oxygen atoms to the lanthanum ion. The peak at 2.8 Å is primarily due to La-Mn scattering, but includes contributions from the La-La/Ca peak at 3.6 Å. As the calcium concentration is increased from 0.12 to 0.25, the La-O environment appears unchanged. Indeed, a simulation of LaMnO$_3$ shows a very similar La-O distribution near 1.8 Å [Fig. 11(c)]. At the three lower doping ranges, the biggest changes are in the La-La/Ca peak at 3.6 Å. This change is expected, since Ca is a much weaker backscattering atom than La. The changes in the La-Mn peak at 2.8 Å are at least partially explained by overlap with the La-La peak. This La-Mn peak is less distorted than the simulation of LaMnO$_3$ would suggest, just as for the Mn-La/Ca peak in the Mn K-edge data. The $x=0.65$ sample is different than the others: The La-O amplitude is larger (indicating less distortion) as is the La-Mn peak, while the La-La/Ca peak is not discernible in the transforms.

The simulation in Fig. 11(c) is calculated using the orthorhombic unit cell from Ref. 40. This unit cell appears to compare a bit more favorably to the nominally orthorhombic
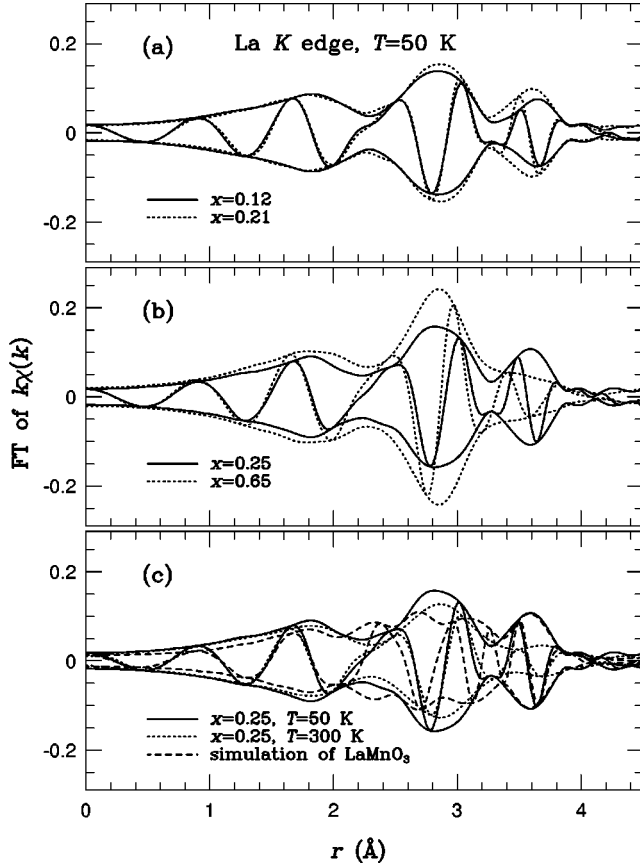
FIG. 11. La K-edge FT of $k\chi(k)$ vs r. Panels (a) and (b) show data for $x=0.12$, 0.21, 0.25, and 0.65 at $T=50$ K. The biggest changes with x occur for the peak at 3.6 Å, which is predominantly due to La-La and La-Ca atom pairs. The La-O distribution does not change appreciably with x. Panel (c) shows data for $x=0.25$ at both 50 K and 300 K. The amplitude of the La-O peak changes only slightly over this temperature range, while the La-La/Ca peak changes more abruptly. Also shown is a simulation of the La K edge of LaMnO$_3$, calculated using diffraction data from Norby *et al.* (Ref. 40).

Ca-doped manganites for the nearest-neighbor La-O peak than the monoclinic cell used in Ref. 41 and Fig. 4.

The La-O widths ($\sigma_{\text{La-O}}^2$) as a function of temperature are shown in Fig. 12. The widths of most of the data are very similar and increase very slowly with temperature, with no correlation to the magnetization. The only exception is the $x=0.65$ sample, which has a stronger temperature dependence. This result will be discussed in Sec. IV D. In any case, the increase in disorder seen in the Mn-O pairs associated with the magnetization is not present in the La-O pairs. Since these pairs are roughly perpendicular to each other, these measurements show that the extra disorder in the Mn-O bonds is mostly in the direction of those bonds and has little if any component perpendicular to that direction. Similarly, no change in the mean La-O bond lengths was observed within ~ 0.015 Å (not shown). Since the Mn-La/Ca distribution has been shown to not change significantly near T_c (Ref. 26) (these data agree), we may therefore limit any possible change in the Mn-O-Mn bond angle near T_c to $\sin^{-1}(0.015/1.9) \cong 0.5°$.
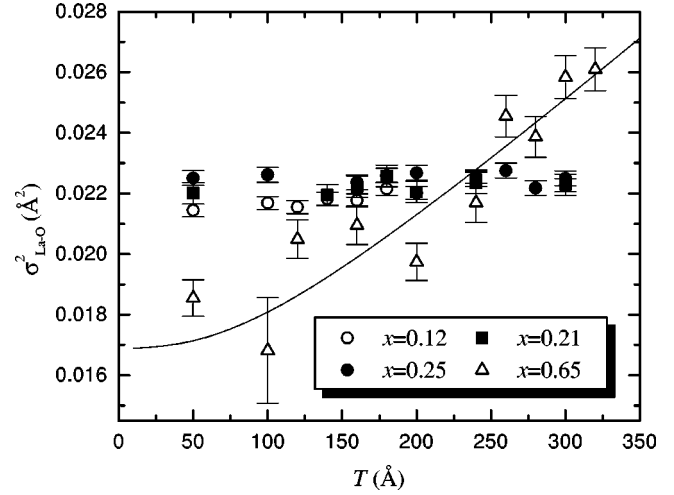

FIG. 12. $\sigma_{\text{La-O}}^2$ vs T for $x=0.12$, 0.21, 0.25, and 0.65. The distortions in the La-O peak are modeled by a single harmonic distribution, similarly to the fits of the Mn K-edge XAFS data. The FM samples show very little temperature dependence, although estimated errors allow for a Θ_D as small as 900 K. The $x=0.65$ σ^2's increase more rapidly, consistent with $\Theta_D = 425 \pm 50$ K.

IV. DISCUSSION AND ANALYSIS

A. MnO$_6$ distortion in the paramagnetic state: Jahn-Teller, charge disproportionation, or isotropic polaron distortions?

The primary results described above are that the MnO$_6$ octahedra are distorted for $x \neq 1$ and that this distortion is mostly, but not completely, removed below T_c in the CMR samples. The presence of the distortion at high temperatures is evidence for a lattice polaron, which becomes partially delocalized as the sample becomes ferromagnetic. The existence of such polaron distortions has been well established.[24–27] However, the symmetry of the experimentally observed polarons and the connection with the JT effect have not been thoroughly addressed. Identifying the nature, i.e., the cause, of the measured distortions is an important step towards understanding the physics of the La$_{1-x}$Ca$_x$MnO$_3$ series. Here, we examine the possibility that distortions are caused by the Jahn-Teller effect or by some other distorting mechanism.

1. Possible models for the Mn-O distortion

First, consider the different models and how they should manifest themselves in the structure. For simplicity, we will assume that above T_c, the electrons are well localized, and thus individual Mn^{3+} and Mn^{4+} sites exist throughout the crystal. In a JT distortion, each Mn^{3+} site will have a distribution of two oxygen atoms ~ 1.9 Å away, two ~ 1.97 Å away, and two about 2.15 Å away, as in LaMnO$_3$. At the same time for $x \neq 0$ in La$_{1-x}$Ca$_x$MnO$_3$, there will be $6x$ Mn^{4+}-O bonds at ~ 1.9 Å per unit cell, as in CaMnO$_3$. If there is no JT distortion, one expects to have a bond length distribution given roughly by the sum of the radii of whatever Mn ions are present and the oxygen atomic radii. If CD (charge disproportionation) occurs, one will expect some number of Mn^{2+}-O bonds at ~ 2.18 Å, some Mn^{+3}-O bonds at 1.99 Å, and some Mn^{4+}-O bonds at 1.88 Å (using radii

from Ref. 46). Of course, lattice effects are not really included by merely summing atomic radii. For instance, the small atomic radii of Ca and La cause the Mn-O-Mn bond angle to be smaller than 180°. If one includes lattice effects for the Mn^{3+}-O bonds, one might expect it to be more like the intermediate bond in LaMnO$_3$, that is, 1.97 Å long. Likewise, Mn^{4+}-O bonds in this structure should be more like 1.90 Å, as in CaMnO$_3$. In any case, the reader should notice immediately that practically the same bond lengths occur in this model as in the JT distortion. Therefore, it is not enough to show that long Mn-O bonds exist around 2.15 Å to say that the distortion is caused by the JT effect. Moreover, polaron distortions in the *absence* of JT or CD effects will still produce distortions that could change with magnetization. For instance, a well-localized charge will cause a symmetric distortion of oxygen around it, i.e., a breathing-mode distortion. In this model, which we refer to as the ionic polaron (IP) model, all Mn^{3+}-O bond lengths would be ~ 1.97 Å and all Mn^{4+}-O bond lengths would be ~ 1.90 Å. In order to differentiate between these possibilities, we will exploit how these models differ with changing x, and how they should change when the distortion is partially removed by a finite magnetization.

2. Discerning between distortion models

Now consider the XAFS data above T_c. Recall that the basic mechanism of transport above T_c is well established to be activated hopping.[22,23] In this temperature regime, the hopping frequency is impeded by the lack of a DE channel, since the samples are merely paramagnetic. The slow hopping frequency allows the lattice to relax around the well-localized charge carrier, forming a small polaron, i.e., well-defined distortions. What is the symmetry of this distortion? The data presented in Fig. 6 give us a strong clue regarding this question. The amplitude shown in Fig. 6 is inversely proportional to the distortion of the MnO$_6$ octahedra. Since the Mn-O environment in the doped samples acts like a linear combination of the end compounds, the magnitude of the distortions is fully consistent with a model where the Mn that are closely associated with La neighbors undergo a JT distortion while the others do not. In the real material, Mn associated with both Ca and La atoms probably has intermediate distortions, and therefore the actual pair-distribution function may be "quasicontinuous."

Neither CD nor IP models would behave this way. A CD model has all the correct bond lengths (as mentioned above); however, the degree to which Mn^{3+} must disproportionate in order to explain the thermogravimetric analysis[31,32] (TGA) and TEP (Ref. 33) results must change significantly with calcium concentration. In fact, the effect is supposed to be large ($\sim 80\%$) in LaMnO$_3$. This notion is already suspect, since if CD does occur to any significant degree, the relative number of intermediate-length bonds (~ 1.97 Å) would be decreased, and diffraction analyses invariably show that $\sim 1/3$ of the Mn-O bonds in LaMnO$_3$ are ~ 1.97 Å. (Diffraction experiments should provide the most accurate information for the pure materials, where structures are most likely periodic.) However, even if we consider LaMnO$_3$ as anomalous, the TGA and TEP data also require that the CD effect gradually become smaller with increasing x, and should disappear at 45% calcium concentration. Therefore, in this

model, the Mn-O bond length distribution would not be a simple linear combination of the end compounds. Rather, it would appear more distorted (fewer intermediate Mn-O bond lengths) at low x, and would order more quickly with x up to $x=0.45$ than one would expect from a linear interpolation between the LaMnO$_3$ and CaMnO$_3$ structures. If the remaining Mn^{3+} ions (the ones that do not disproportionate into Mn^{2+} and Mn^{4+}) also undergo a JT distortion (which we will refer to as CD+JT), we would expect a similar dependence of the distortion on x, but the curve will be offset, agreeing with a JT distortion above $x=0.45$. Last, if the distortions are only due to an IP, the distortion should actually increase with x for small x. [The IP model is already ruled out by diffraction studies of LaMnO$_3$ (Refs. 40 and 41) and PDF studies of La$_{1-x}$Sr$_x$MnO$_3$ (Ref. 27) that show a long Mn-O bond ~ 2.15 Å, but we include the model for completeness.]

To quantify how the different model distortions would affect the XAFS amplitudes, we used FEFF6 to simulate the change in the amplitude for a given model vs the JT-distorted LaMnO$_3$ model (Fig. 6). For instance, if we take a CD model for LaMnO$_3$ at 50 K (no JT distortions), in which 80% of the Mn^{3+}-O (1.97 Å) bonds are converted to Mn^{4+}-O (1.9 Å) and Mn^{2+}-O (2.15 Å) bonds, then we calculate an amplitude that is 86% of the amplitude in the JT model. If we also allow the 20% remaining Mn^{3+} to JT distort, then the amplitude is only 65% of the amplitude of a JT model. At $x=0.3$, we have at least 30% Mn^{4+} from the Ca doping. Performing the same kind of simulation, we find that the CD amplitude would be much larger than given by the JT model ($\sim 113\%$). We have also plotted in Fig. 6 the decreasing amplitude with x for the IP model (at low x). At $x=0.45$, the CD and IP models come together, and for higher x go to the amplitude for CaMnO$_3$. The CD+JT model becomes the JT model above $x=0.45$. Figure 6 shows that the Mn-O peak amplitude vs x in the CD or the CD+JT model increases much more rapidly with x than in a JT model. A measurement of this increased slope would be well within the noise of our experiment. Therefore, the linear character and the rate of change with x of the experimental amplitudes in Fig. 6 rule out the CD, CD+JT, and IP models as the primary cause of the distortions.

From this analysis, we must conclude (in the absence of other sensible models) that the distortions measured above T_c are due to local JT distortions around Mn^{3+} ions. These JT distortions exist across the entire Ca-doping range, including the charge-ordered region, in agreement with the interpretation of Ramirez et al.[5] from thermodynamic and electron diffraction data. We do not have an alternate model for the TGA (Refs. 31 and 32) or TEP (Ref. 33) data.

This analysis depends on the changes of the Mn-O FT peak amplitude with x to make the above conclusions. Note that a CD model in which the fraction of Mn^{3+} disproportionating remains a constant (between 60% and 75%) amount with changing x cannot be ruled out by these data. Likewise, in a CD+JT model, if the CD occurs $\lesssim 10\%$ of the time, these data would not be sensitive. Since diffraction clearly shows a JT distortion in LaMnO$_3$, we conclude that the maximum amount of CD is $\sim 10\%$.

B. Differences in the local structure between the magnetic and paramagnetic states

The character of the distortion changes as the temperature is dropped below T_c. As seen previously,[24–27] the distortion

of the Mn-O distribution decreases commensurate with the increasing magnetization. In addition, we measure an increase in the weighted average Mn-O bond length in the FM state (Fig. 9). Since XAFS is more sensitive to the nearest-neighbor Mn-O bonds (as discussed in Sec. III C), this change in the Mn-O bond length is more consistent with the removal of the JT distortion than a change in random disorder.

The Mn-O bond length data for LaMnO$_3$ are anomalous (i.e., a decrease in the weighted average bond length) in that they seem to indicate that the JT distortion grows with increasing temperature. Although there are fewer data points in the vicinity of $T_N(\sim 130$ K), it is possible that the primary change in the Mn-O weighted bond length occurs at T_N. If we apply the same model for this sample as for the ferromagnetic samples, then this result for LaMnO$_3$ may indicate local ferromagnetic ordering coupling to the JT distortion. Indeed, the magnetic structure is ferromagnetic in planes and antiferromagnetic between planes of Mn and O.[1] However, in order to have a double-exchange coupling, there need to be holes available to make Mn^{4+} sites, and in this material, there should be very few (~ 0.012/unit cell from TGA of oxygen concentration). If a small amount of CD occurs ($\lesssim 10\%$ by the arguments above), enough holes may be available. A temperature-dependent diffraction analysis may help explain this unexpected result.

An important question not adequately addressed by previous works is whether the oxygen moves perpendicularly to the direction of the Mn-Mn pairs at T_c, that is, whether the distortion is caused by a change in the Mn-O-Mn bond angle. Indeed, the magnitude of the Mn-O-Mn bond angle has been related to the hopping matrix element via the effect of the average ionic radius of the La site on T_c.[34] A simple polaron or JT distortion would be along the direction of the neighboring Mn, roughly preserving the Mn-O-Mn bond angle, whereas some distortion of the La/Ca-O bonds would not preserve this angle. These (Fig. 10) and previous XAFS experiments[26] measure a change in the order of the Mn-Mn peak in the FT of $k\chi(k)$ as the temperature passes through T_c, which could have either been due to changes in the Mn-Mn pair distribution or to changes in the Mn-O-Mn bond angle. The La K-edge data reported here now rule out any change in the Mn-O-Mn bond angle within $0.5°$ by observing no change within 0.015 Å in the La-O pair distribution near T_c, either in the distribution width or in the bond length.

The measured changes in the disorder of the Mn-Mn contribution to the XAFS can now be unambiguously attributed to removal of a distortion of the Mn-Mn pairs below T_c (as in the MnO$_6$ octahedra). Moreover, the data showing changes in the disorder of the insulating $x=0.12$ sample near T_c can now be taken to include changes in the Mn-O and the Mn-Mn distribution widths, and perhaps also in the Mn-O weighted bond length. These data are thus strong evidence that DE couples to the lattice distortions even in an insulating (but FM) sample. From Fig. 8, we estimate that the static JT distortion is reduced by ~ 0.02 Å (σ's add in quadrature) in the FM state. This result is consistent with measurements on the La$_{1-x}$Sr$_x$MnO$_3$ series by Louca *et al.*[27]

C. Delocalization and magnetization

At $T=50$ K, the magnetization is virtually saturated (Fig. 1) and the σ's are no longer changing much with temperature
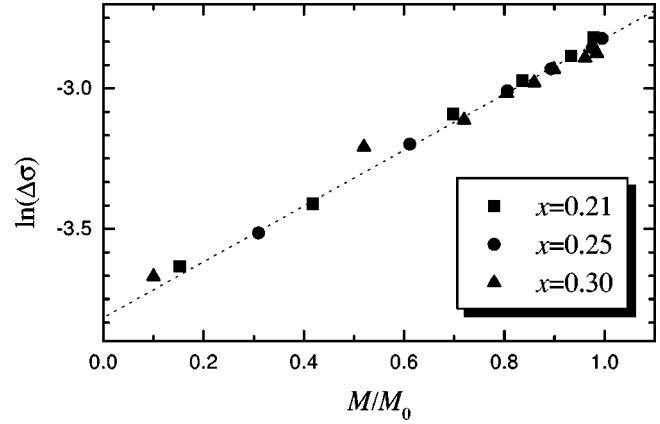

FIG. 13. Natural logarithm of the size of the distortion removed by the magnetization $\Delta\sigma$ [Eq. (1)] vs magnetization (normalized to M at 5 K). All data are described by the equation $\ln(\Delta\sigma) = 0.99(3)M/M_0 - 3.82(5)$.

(Figs. 8, 10, and 12). As shown in Fig. 7, the Mn-O environment in the insulating materials still acts like a linear interpolation of CaMnO$_3$ and the JT-active LaMnO$_3$ Mn-O environments, and therefore the JT distortions are still present. The CMR materials have a smaller distortion, although not as small as one expects by complete removal of the distortion. These data suggest that the distortion and the magnetization may be functionally related. We can estimate the amount of distortion removed by the sample magnetization by extrapolating a curve (from the correlated Debye model) through the high-temperature data for σ^2_{Mn-O} in Fig. 8 and taking the difference:

$$\Delta\sigma^2 = \sigma^2_T + \sigma^2_{FP} - \sigma^2_{Mn-O}, \quad (1)$$

where σ^2_T is the thermal contribution (estimated from a fit to the CaMnO$_3$ data), σ^2_{FP} is the fully developed polaron distortion (estimated at room temperature), and σ^2_{Mn-O} is the data shown in Fig. 8. We have found the $\ln(\Delta\sigma)\propto M/M_0$, and that the data for $x=0.21$, 0.25, and 0.30 all fall on the same line (Fig. 13).

This relationship could be an important clue for understanding the nature of distortions and the transport in the metallic state. Here we consider some simple models of the distortion and try to relate them to the magnetization. The persistence of the distortion in the metallic state suggests that at least some of the electrons causing the polaron distortion are still partially localized on the time scale of phonon vibrations, in agreement with PDF data on La$_{1-x}$Sr$_x$MnO$_3$ (Ref. 27) and with measurements of the magnetic correlation length.[47] This partial localization may be characterized in several ways. One possibility is that if some fraction of the electrons become trapped, then the lattice may have time to relax into a JT distortion around those Mn^{3+} sites. This situation could easily arise if some defect was encountered, such as a Mn^{2+} ion or a Mn vacancy. We will call this model the ''two-fluid'' model, since some holes will be localized and others will be delocalized charge carriers. In this case the distortions on the localized sites are essentially static.

A second possibility is that all the charge carriers in the metallic state are partially delocalized, creating an ''average,'' essentially static, distortion over several unit cells.[27]

We refer to this model as the extended polaron model. A third possibility is that the systems are in an intermediate regime in which the hopping frequency is enhanced by the DE:[16–19] Here, the distortion can *partially* relax before the next hop occurs and we would measure only a partial removal of the distortion.[48] The remaining distortions are then better characterized as dynamic disorder, since locally the Mn-O bond lengths are time dependent, and the bond length distribution would be continuous.

Although these different transport possibilities all have distinctly different Mn-O bond length distributions, the sensitivity of current local structure probes cannot differentiate between them. However, we can model at least the two-fluid model and the extended polaron model and consider how they might scale with the magnetization.

We will now consider these models and how they should affect the XAFS results, beginning with the two-fluid model. The linear dependence of the distortion on the calcium concentration (Figs. 6 and 7) suggests that the amplitude of the Mn-O peak is a good predictor of the localized hole concentration. Below T_c, a large fraction of the holes in the CMR samples become delocalized (Fig. 7). As a model of this distortion, consider the effect of removing the distortion around some fraction of the manganese sites. In this model, the pair-distribution function (which is proportional to the FT amplitude for relatively small distortions) is the sum of two (unresolved) Gaussians, centered on approximately the same average bond length. Gaussian $G1$ represents the Mn ions with nearly itinerant charge carriers; it has a narrower width than Gaussian $G2$, which represents Mn atoms with localized polarons. The fractional weight of these two Gaussians changes with the magnetization, which in turn changes the overall peak amplitude of the sum: $A_{total} = A_{G1} + A_{G2}$. Therefore, assuming that the Mn-O peak amplitude is a good measure of the localized hole concentration below as well as above T_c, we can measure the *delocalized* hole concentration n_{dh} in terms of the available holes x as:

$$n_{dh} = \frac{A(x,T,M) - A_D(x,T)}{A_{ND}(x,T) - A_D(x,T)} x,$$ (2)

where $A(x,T,M)$ is the total peak amplitude of the pair-distribution function at some magnetization M, $A_D(x,T)$ is the peak amplitude if the distortion were fully developed, and $A_{ND}(x,T)$ is the amplitude if there were no distortion of the peak. Since $A \propto 1/\sigma$, we can use the width measurements obtained in the fits, yielding

$$n_{dh} = \frac{1/\sigma_{Mn\text{-}O} - 1/\sigma_D}{1/\sigma_{ND} - 1/\sigma_D} x.$$ (3)

The width with no distortion σ_{ND} is the temperature-dependent contribution σ_T. The width from a fully distorted Mn-O distribution σ_D is given by the thermal contribution and the additional disorder from a fully developed polaron distortion σ_{FP}: $\sigma_D^2 = \sigma_{FP}^2 + \sigma_T^2$. As mentioned above, σ_{FP} is a constant that we determine from the room temperature data.

To lowest order, $\Delta\sigma^2 \propto n_{dh}$, and so it is not surprising that we find that n_{dh} as calculated from Eq. (3) depends exponentially on the magnetization for the CMR samples, as shown in Fig. 14. Each line is described well by the function
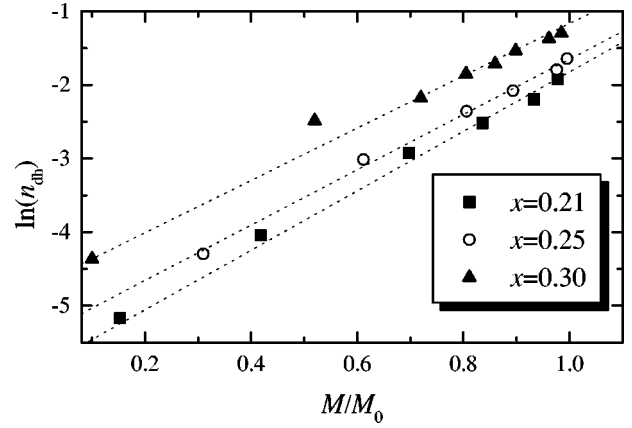

FIG. 14. Natural logarithm of the modeled delocalized hole concentration n_{dh} vs magnetization (normalized to M at 5 K). n_{dh} is calculated using only the MnO$_6$ distortions [Eq. (3)], yet has a similar functional dependence on the magnetization as the resistivity (Ref. 22).

$$n_{dh} = n_0(x) \exp\left[K_n \left(\frac{M}{M_0} - 1 \right) \right].$$

This form of the equation is chosen so that $n_0(x)$ gives the (maximum) number of delocalized holes at $M = M_0$; estimated values are $n_0(x) = 0.16(2)$, $0.19(2)$, and $0.26(2)$ for $x = 0.21$, 0.25, and 0.30. The coefficient K_n appears to be a constant in this small sample set, $K_n = 3.8 \pm 0.2$. At low temperatures, the fractional number of holes, $F = n_0/x$, does not reach unity (as expected from Fig. 7), with ~20% of the holes still localized. The data indicate that F increases from ~77% to 86% from $x = 0.21$ to 0.30. It would be interesting to determine F for a finer grid of calcium concentrations from $x \approx 0.2$ to 0.48 and measure the concentration where F is maximized. Reference 27 indicates that in the Sr material, $F = 1$ for CMR samples with $x \gtrsim 0.35$.

In simple transport models, $\rho = 1/(ne\mu_c)$, where μ_c is the effective carrier mobility and n is the number of charge carriers per unit volume. Therefore, transport measurements showing $\rho \propto \exp(-K_\rho M/M_0)$ (Ref. 22) are essentially in agreement with the data shown in Fig. 14. One might expect the factor K_ρ to be equal to our measurement of K_n. However, in the units used in this paper, we estimate $K_\rho = 5.2 \pm 0.3$ from Ref. 22. This difference may be due to a sample-dependent effect but is more likely the result of μ_c changing with M or T. A combination of the structural and transport measurements can produce the following interesting result, based on the conjecture that the results for K_ρ are not very sample dependent. (This conjecture is not unreasonable, since the K_n are roughly constant for the three samples measured in this study.) Since the structural measurement of the delocalized hole concentration n_{dh} is not dependent on the mobility μ_c (at least according to this model), $K_n < K_\rho$ may indicate that μ increases with increasing M. If so, the combination of this structural measurement with the transport measurements suggests

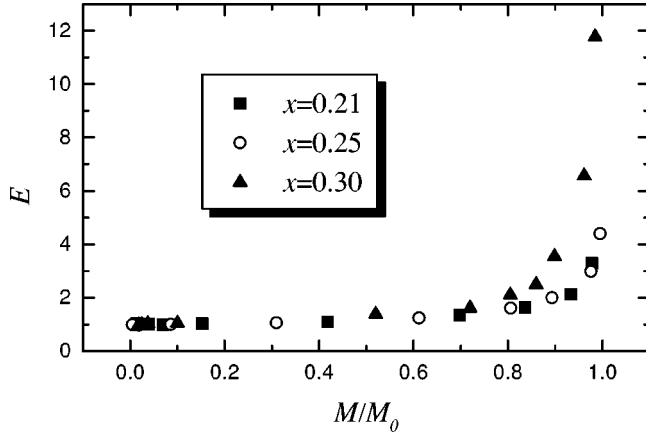$$\mu_c \propto \exp\left(K_\mu \frac{M}{M_0} \right),$$

FIG. 15. The modeled extent E [Eq. (4)] of the polaron distortion per available hole x vs the normalized magnetization (normalized to M at 5 K).

with $K_\mu = 1.4 \pm 0.4$. A measurement of the Hall mobility vs M could help determine whether or not the model used to determine n_{dh} [Eq. (2)] should somehow include μ_c. Unfortunately, Hall measurements on magnetic samples with large magnetoresistance effects are very difficult to interpret.

The model for the delocalized hole concentration used in Eq. (2) assumes that a delocalized hole no longer contributes at all to the MnO_6 distortions; i.e., it becomes completely itinerant. Increasing the magnetization would ''release'' holes into the conducting state. This model is functionally the same as used by Hundley *et al.*,[49] which explains the $\rho \propto \exp(-K_\rho M/M_0)$ relation in terms of a decreasing polaron binding energy W_p with increasing M. Using this comparison, the W_p is directly related to the distortion.

Of course, as mentioned above, other models may also be able to explain the essential physics and how the distortions scale with the magnetization. Another model that may describe the transport is the extended polaron model. This model ascribes the change in the distortion to a charge that is spread out over more than one site. In this picture, the distortion is reduced proportionally to the number of Mn sites (or extent E) included within the polaron generated by a single, partially delocalized hole. An estimate for E is obtained from

$$E = \frac{A_{ND}(x,T) - A_D(x,T)}{A_{ND}(x,T) - A(x,T,M)}. \qquad (4)$$

Figure 15 shows E as a function of the magnetization. From this equation we would infer that at low temperatures, the polaron is spread out over three to five Mn sites (possibly more for the $x=0.30$ sample). However, a plot of $\ln(E)$ vs M does not produce a straight line, and we are not clear how *a priori* to relate this quantity to transport measurements.

Although the two-fluid model fits the data well and agrees with transport measurements, the apparent independence of the curves in Fig. 13 of x is still unexplained. The actual transport mechanism may be better explained by an intermediate coupling of the carriers to the lattice with a double-exchange interaction.[16–19] A calculation of the magnitude of the Mn-O distortions within these models as a function of M

has not been explicitly performed, as far as we know. However, such a calculation is implicitly included in the models.

D. Incommensurate to commensurate charge ordering transition in $La_{0.35}Ca_{0.65}MnO_3$

The distortions of the first Mn-O peak for $x=0.65$ are consistent with all the other samples measured, in that the distortion can be modeled as a JT distortion around available Mn^{3+} ions and no distortion around Mn^{4+} ions (Figs. 6 and 7), within the resolution of these XAFS experiments. This distortion is maintained at all temperatures; the measured width of the pair distribution is almost independent of temperature and can be fit to a Debye model with a rather high Debye temperature with static disorder. Although we have no electron diffraction data demonstrating that this sample charge orders, we do see changes in the magnetization with temperature that are consistent with the formation of the charge-ordered state.[5] Even so, it is likely that the local Mn-O structure is only weakly sensitive to this state, since the excess charge remains localized both above and below T_N. Rather than delocalizing as in the CMR materials, the location of the doped charges becomes periodic. Our measurements indicate that any possible changes in the Mn-O widths σ^2 either at T_N or T_{CO} are limited to 0.0002 Å^2. A similar lack of change in the local structure has been shown to occur at the ferroelectric transition in $PbTiO_3$.[50]

In terms of the nearest-neighbor structure, the only interesting difference between this sample and the other insulating samples is that the correlated Debye temperature Θ_D is much higher for the $x=0.65$ Mn-O pairs (~ 1100 K) than for the other samples, which all have $\Theta_D \lesssim 940$ K in the insulating state. This large Θ_D for $x=0.65$ is also at odds with the measurement of $\Theta_D = 950$ K for the Mn-O distribution in an AF sample of $La_{0.5}Ca_{0.5}MnO_3$,[26] which shows signs of CO in the magnetization curves as well. The large value of Θ_D is surprising for this substituted sample, as one would expect the strongest bonds to be found in the highly ordered $CaMnO_3$ material. The much weaker temperature dependence of σ^2 in the 65% sample may be related to additional disorder in the CO state below T_N. For instance, although the data fit a thermal model well (but with an unusually high Debye temperature), there may also be a combination of both thermal and other effects that conspires to produce the observed very weak temperature dependence. However, futher data are needed to explore this possibility.

In contrast, the temperature dependence of σ^2 for the La-O pair distribution is weak for the FM samples but quite strong for the 65% sample: That is, Θ_D is much higher in the FM samples (>900 K; see Fig. 12) than for the $x=0.65$ sample (~ 425 K). These CO systems therefore merit further study.

V. CONCLUSION

We have reported XAFS data that clarify the nature of the distortions in the $La_{1-x}Ca_xMnO_3$ materials. Comparisons of the Mn-O distribution above T_c for various x show that the Mn-O distortions are consistent with a linear interpolation of the end-member compounds $LaMnO_3$ and $CaMnO_3$, indicating that proposed charge disproportionation models are in-

consistent with the local structure. By contrast, a model which includes a Jahn-Teller distortion in proportion to the Ca concentration fits the data well. Below T_c, this linear interpolation fails for samples exhibiting a CMR effect as the disorder in Mn-O pairs is reduced, consistent with pair-distribution function analyses.[24,27] However, the Mn-O peak amplitudes are still not completely ordered, indicating that the polarons may not be completely delocalized (consistent with Ref. 27 for the Sr compounds). This result is supported by the lack of a significant shift in the Mn K-edge threshold energy, in agreement with Subías et al.[39] Small changes in the weighted average Mn-O bond length through T_c show that the change in disorder is not symmetric about Mn, consistent with a change in a JT distortion. We also report La K-edge data that indicate that any change in the Mn-O-Mn bond angle around T_c is limited to $<0.5°$. This result shows that changes in $\sigma_{\text{Mn-Mn}}$ are along the Mn-O bonds; consequently, the Mn atoms are displaced as well as the O atoms. The combination of all these results indicates that the essential physics is described by local JT distortions above T_c that are partially delocalized below T_c, although small amounts of CD ($\lesssim10\%$) cannot be ruled out. These distortions scale with transition temperature and magnetization. In particular, by using a model that equates the removal of the JT distortion around a single Mn site with the creation of a delocal-

ized hole n_{dh}, we find that $\ln(n_{\text{dh}})\propto M$. Since $\ln(\rho)\propto-M$ and, in simple transport models, $\rho\propto1/n\mu_c$ (n is the number of charge carriers, and μ_c is the mobility), we now have empirical relations between the spin, charge, mobility, and lattice distortions in the CMR perovskites.

---

*Permanent address: Los Alamos National Laboratory, MS K764, Los Alamos, NM 87545.

†Permanent address: Physics Department, Florida Atlantic University, Boca Raton, FL 33431.

[1] E. O. Wollan and W. C. Koehler, Phys. Rev. **100**, 545 (1955).

[2] G. H. Jonker and J. H. van Santen, Physica (Amsterdam) **16**, 337 (1950).

[3] G. H. Jonker, Physica (Amsterdam) **22**, 707 (1956).

[4] P. Schiffer, A. Ramirez, W. Bao, and S-W. Cheong, Phys. Rev. Lett. **75**, 3336 (1995).

[5] A. P. Ramirez, P. Schiffer, S-W. Cheong, C. H. Chen, W. Bao, T. T. M. Palstra, P. L. Gammel, D. J. Bishop, and B. Zegarski, Phys. Rev. Lett. **76**, 3188 (1996).

[6] C. H. Chen, S-W. Cheong, and H. Y. Hwang, J. Appl. Phys. **81**, 4326 (1997).

[7] J. Volger, Physica (Amsterdam) **20**, 49 (1954).

[8] C. Zener, Phys. Rev. **82**, 403 (1951).

[9] P. W. Anderson and H. Hasegawa, Phys. Rev. **100**, 675 (1955).

[10] P. G. de Gennes, Phys. Rev. **118**, 141 (1960).

[11] R. M. Kusters, J. Singleton, D. A. Keen, R. McGreevy, and W. Hayes, Physica B **155**, 362 (1989).

[12] K. Chahara, T. Ohuo, M. Kasai, and Y. Kozono, Appl. Phys. Lett. **63**, 1990 (1993).

[13] R. von Helmolt, J. Wecker, B. Holzapfel, L. Schultz, and K. Samwer, Phys. Rev. Lett. **71**, 2331 (1993).

[14] S. Jin, M. McCormack, T. H. Tiefel, R. M. Fleming, J. Phillips, and R. Ramesh, Science **264**, 413 (1994).

[15] A. J. Millis, P. B. Littlewood, and B. I. Shraiman, Phys. Rev. Lett. **74**, 5144 (1995).

[16] H. Röder, J. Zang, and A. R. Bishop, Phys. Rev. Lett. **76**, 1356 (1996).

[17] A. J. Millis, B. I. Shraiman, and R. Mueller, Phys. Rev. Lett. **77**, 175 (1996).

[18] A. J. Millis, Phys. Rev. B **53**, 8434 (1996).

[19] A. J. Millis, R. Mueller, and B. I. Shraiman, Phys. Rev. B **54**, 5405 (1996).

[20] A. Asamitsu, Y. Moritomo, Y. Tomioka, T. Arima, and Y. Tokura, Nature (London) **373**, 407 (1995).

[21] G. Zhao, K. Conder, H. Keller, and K. A. Müller, Nature (London) **381**, 676 (1996).

[22] M. F. Hundley, M. Hawley, R. H. Heffner, Q. X. Jia, J. J. Neumeier, J. Tesmer, J. D. Thompson, and X. D. Wu, Appl. Phys. Lett. **67**, 860 (1995).

[23] M. Jaime, M. B. Salamon, K. Pettit, M. Rubinstein, R. E. Treece, J. S. Horwitz, and D. B. Chrisey, Appl. Phys. Lett. **68**, 1576 (1996).

[24] S. J. L. Billinge, R. G. DiFrancesco, G. H. Kwei, J. J. Neumeier, and J. D. Thompson, Phys. Rev. Lett. **77**, 715 (1996).

[25] T. A. Tyson, J. Mustre de Leon, S. D. Conradson, A. R. Bishop, J. J. Neumeier, and J. Zang, Phys. Rev. B **53**, 13 985 (1996).

[26] C. H. Booth, F. Bridges, G. J. Snyder, and T. H. Geballe, Phys. Rev. B **54**, R15 606 (1996).

[27] D. Louca, T. Egami, E. L. Brosha, H. Röder, and A. R. Bishop, Phys. Rev. B **56**, R8475 (1997).

[28] P. Dai, J. Zhang, H. A. Mook, S.-H. Liou, P. A. Dowben, and E. W. Plummer, Phys. Rev. B **54**, 3694 (1996).

[29] P. Dai, J. Zhang, H. A. Mook, F. Foong, S-H. Liou, P. A. Dowben, and E. W. Plummer, Solid State Commun. **100**, 865 (1996).

[30] G. H. Kwei, D. N. Argyriou, S. J. L. Billinge, A. C. Lawson, J. J. Neumeier, A. P. Ramirez, M. A. Subramanian, and J. D. Thompson, in *Magnetic Ultrathin Films, Multilayers, and Surfaces*, edited by D. D. Chambliss, J. G. Tobin, D. Kubinski, K. Barmak, W. J. M. de Jonge, T. Katayama, A. Schuhl, and P. Dederichs, MRS Symposia Proceedings No. 475 (Materials Research Society, Pittsburgh, 1997), p. 533.

[31] J. A. M. van Roosmalen and E. Cordfunke, J. Solid State Chem. **110**, 109 (1994).

[32] J. A. M. van Roosmalen and E. Cordfunke, J. Solid State Chem. **110**, 113 (1994).

[33] M. F. Hundley and J. J. Neumeier, Phys. Rev. B **55**, 11 511 (1997).

[34] H. Hwang, S-W. Cheong, P. Radaelli, M. Marezio, and B. Batlogg, Phys. Rev. Lett. **75**, 914 (1995).

[35] J. L. Cohn, J. J. Neumeier, C. P. Popoviciu, K. J. McClellan, and T. Leventouri, Phys. Rev. B **56**, R8495 (1997).

[36] C. H. Booth, F. Bridges, G. H. Kwei, J. M. Lawrence, A. L. Cornelius, and J. J. Neumeier, Phys. Rev. Lett. **80**, 853 (1998).

[37] S. I. Zabinsky, J. J. Rehr, A. Ankudinov, R. C. Albers, and M. J. Eller, Phys. Rev. B **52**, 2995 (1995).

[38] G. G. Li, F. Bridges, and C. H. Booth, Phys. Rev. B **52**, 6332 (1995).

[39] G. Subías, J. García, M. G. Proietti, and J. Blasco, Phys. Rev. B **56**, 8183 (1997).

[40] P. Norby, I. G. Krogh Andersen, E. Krogh Andersen, and N. H. Andersen, J. Solid State Chem. **119**, 191 (1995).

[41] J. F. Mitchell, D. N. Argyriou, C. D. Potter, D. G. Hinks, J. D. Jorgensen, and S. D. Bader, Phys. Rev. B **54**, 6172 (1996).

[42] K. R. Poeppelmeier, M. E. Leonowicz, J. C. Scanlon, and J. M. Longo, J. Solid State Chem. **45**, 71 (1982).

[43] B. F. Woodfield, M. L. Wilson, and J. M. Byers, Phys. Rev. Lett. **78**, 3201 (1997).

[44] J. B. Elemans, B. van Laar, K. J. R. van der Veen, and B. O. Loopstra, J. Solid State Chem. **3**, 238 (1971).

[45] A note about anharmonic distortions: In XAFS analysis, if a pair distribution has a significant third moment, that is, if the distribution is skewed, then if this moment is not accounted for in the fits, one will measure a false decrease in bond length with temperature [P. Eisenberger and G. S. Brown, Solid State Commun. **29**, 418 (1979)]. These data can be fit with a large third moment of ~ 0.08 Å. However, inclusion of such a moment in the fit does not significantly change any of the results listed above.

[46] R. D. Shannon, Acta Crystallogr., Sect. A: Found. Crystallogr. **32**, 7519 (1976).

[47] J. W. Lynn, R. W. Erwin, J. A. Borchers, Q. Huang, A. Santoro, J.-L. Peng, and Z. Y. Li, Phys. Rev. Lett. **76**, 4046 (1996).

[48] J. Ranninger and U. Thibblin, Phys. Rev. B **45**, 7730 (1992).

[49] M. F. Hundley, J. J. Neumeier, R. H. Heffner, Q. X. Jia, X. D. Wu, and J. D. Thompson, in *Epitaxial Oxide Thin Films III*, edited by D. G. Schlom, C.-B. Eom, M. E. Hawley, C. M. Foster, and J. S. Speck, MRS Symposia Proceedings No. 474 (Materials Research Society, Pittsburgh, 1997), p. 167.

[50] N. Sicron, B. Ravel, Y. Yacoby, E. A. Stern, F. Dogan, and J. J. Rehr, Phys. Rev. B **50**, 13 168 (1994).